

Article

Effect of Hot-Dip Galvanizing Process on Selective Oxidation and Galvanizability of Medium Manganese Steel for Automotive Application

Zhang Chen ^{1,2}, Yanlin He ^{1,2,*}, Weisen Zheng ^{1,2,*}, Hua Wang ¹, Yu Zhang ³ and Lin Li ^{1,2}

¹ School of Materials Science and Engineering, Shanghai University, Shanghai 200044, China; chenzhangyv@shu.edu.cn (Z.C.); wh225@shu.edu.cn (H.W.); liling@shu.edu.cn (L.L.)

² State Key Laboratory of Advanced Special Steel, Shanghai University, Shanghai 200044, China

³ Ansteel Group Beijing Research Institute, Beijing 102211, China; zhangyu@ansteel.com.cn

* Correspondence: ylhe@t.shu.edu.cn (Y.H.); wszheng@shu.edu.cn (W.Z.)

Received: 2 December 2020; Accepted: 16 December 2020; Published: 21 December 2020



Abstract: A medium manganese steel with 7.5 wt.% Mn for automobile application was galvanized in a continuous Hot Dip Galvanizing (HDG) simulator under different galvanizing conditions. It was shown that the effects of dew point, annealing temperature and annealing atmosphere on the surface oxidation of steel could be comprehensively evaluated by the consideration of oxygen partial pressure $P(\text{O}_2)$. Although Mn_2SiO_4 was a thermodynamic stable phase when $P(\text{O}_2)$ varied from 10^{-28} to 10^{-21} atm, it was difficult to form Mn–Si–O composite oxide because there was no enrichment of silicon on the steel surface. So, this oxide was generally formed in the Fe substrate and had little effect on the galvanizability. With the increase in $P(\text{O}_2)$ above 10^{-25} atm, MnO particles in the form of the thermodynamic stable phase became coarser and tended to aggregate, which hindered the formation of a continuous inhibition layer, resulting in the defects of bare spots on the galvanized surface of the steel. When the oxygen partial pressure greater than 10^{-22} atm, film-like MnO layer was formed on the surface of steel sample, which obviously deteriorated the galvanizability. The galvanizability of the steel can be improved by the regulation of oxygen partial pressure; based on this, the reasonable zinc plating process parameters can be developed.

Keywords: hot-dip galvanizing process; medium-manganese steel; oxygen partial pressure; galvanizability

1. Introduction

In recent years, the realization of automotive lightweight and high safety is a trend in the development of global automobile industry. As one of the third generation of advanced high strength steel (AHSS), medium manganese steel has received great interest from researchers due to its combination of high strength and plasticity, which is the result of the partition of carbon and manganese composites and the regulation of metastable phases [1–3]. In order to enhance the stability of austenite in medium-manganese steel, alloying elements such as Mn or Si are often added to the steel. However, these alloying elements are easy to be oxidized in the hot-dip galvanizing annealing process. The presence of film-like or granulated SiO_2 and MnO surface oxides lead to deterioration of the reactive wettability of liquid zinc and hindrance of the formation of Fe–Al–Zn inhibition layer, thus worsening the quality of zinc coatings [4–8].

In the previous work, the effects of annealing process and composition on the selective oxidation and galvanizability of advanced high-strength steel were investigated during a continuous hot-dip galvanizing process. Maderthaner et al. [9] showed that for 1.5 Si–2.5 Mn high strength steel at the

dew point of -30 and -58 °C, the segregation of Mn and Si was significantly reduced at the lower dew point. Moreover, the decrease in the dew point could convert the film-like oxides into particles which was helpful in forming a continuous inhibition layer, say, the galvanizability of steel at lower dew point would be better. On the contrary, Mousavi et al. [10] indicated that when the high strength steel with a composition of 0.1 C–2 Mn–1.3 Si was annealed at the dew point of -50 , -30 , and $+5$ °C, the types of oxides formed on the surface were basically the same, but thick film-like oxides were formed on the surface of steel annealed at the dew point of -50 °C, and a large area of bare spots appeared on the galvanized surface of this specimen. The surface quality of other specimen annealed at higher dew point was better. So, it is obviously not enough to consider only the influence of dew point on galvanizability for high strength steels. Recently, Pourmajidian et al. [11–13] studied the effects of annealing temperatures, dew points and composition on the oxidation behavior and reactive wetting of 0.1 C–6 Mn–2 Si steel. However, it was still difficult to find out the key factor that determines the galvanizability of medium manganese steel and develop the reasonable galvanizing process accordingly. Obviously, it could hinder the development and application of medium manganese steel.

Yang et al. [14] combined the experimental analysis and thermodynamic calculation to analyze the effect of oxygen partial pressure on the formation of surface oxides in medium manganese lightweight steel. It seems feasible to evaluate the galvanizability of experimental steel by calculating the variation of oxide under different oxygen partial pressures. Based on this, the selective oxidation and galvanizability of the medium manganese steel, which contains manganese and silicon, with a more complex oxidization behavior were investigated in this work. Moreover, the relationship between the oxygen partial pressure and galvanizability was attempted first to be established, which can obtain the regulation method of the galvanizing process and provide a theoretical reference for industrial production.

2. Materials and Experiments

The hot-dip galvanizing simulation experiment in this work is carried out on the Iwatani Surtec hot-dip galvanizing simulator (Aichi, Japan). In addition, the process conditions for 0.2 C–7.5 Mn–0.2 Si (wt.%) steel used in the galvanizing simulation experiment are listed in Table 1.

Table 1. The annealing process of medium manganese steels.

No.	Annealing Temperature/K	Dew Point/°C	H ₂ Content
1#	873	-10	20%
2#	923	-10	5%
3#			20%
4#	1093	-50	20%
5#		-10	
6#		$+10$	

The steel sheets used in this hot-dip galvanization are cut from the 1.2 mm thick as-received cold-rolled sheets parallel to the rolling direction, with a size of 100 mm × 220 mm. The surfaces of the sheets were washed with acetone and deionized water after the acid picking treatment, and then polished with 4000 grit SiC paper to reduce the negative effect of surface roughness on the subsequent galvanizing process. In this work, steel sheets were heated from room temperature to three different annealing temperatures of 873 K (600 °C), 923 K (650 °C) and 1093 K (820 °C) at a heating rate of 30 K/s, held for 4 min, and subsequently cooled down to the dipping temperature of 733 K (460 °C) at a cooling rate of 20 K/s, respectively. A 1093 K annealing temperature, -10 °C dew point and 20% H₂ are the frequently used parameters on the hot-dip galvanizing production line. Other parameters were set for comparison in experiments, where -50 °C is the lowest dew point that the galvanizing simulator can reach. In addition, the steels annealed at 873 and 923 K have good mechanical properties, with the tensile strength exceeding 1500 MPa and elongation exceeding 15% (the detailed study will be reported

separately). All sheets were immersed in the liquid Zn bath containing 0.2 wt.% Al for 3 s before a final rapid cooling to room temperature.

Anti-rust oil is applied to the surface of galvanized steel sheet to prevent surface oxidation in the subsequent experimental analysis. The dimension of all specimens for microscopic observation is 10 mm × 10 mm. The specimens used to observe the oxidation were cut from the clamping ends which had not been immersed in the zinc bath, while the specimens used to observe the interfacial layer between the zinc coating and matrix were cut from the location covered with zinc coating, which should be removed before the observation. The sampling position is shown in Figure 1.

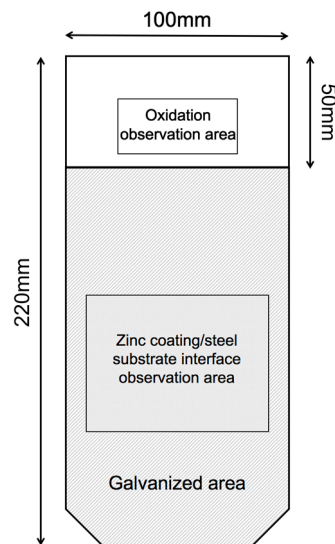


Figure 1. Sampling diagram of galvanizing steel.

In this work, a Hitachi S-570 field emission scanning electron microscope (FE-SEM, Tokyo, Japan) was used to observe the morphology of the oxide and inhibition layer on the surface of specimens, and equipped energy dispersive spectroscopy (EDS) was used to analyze the surface elements. Bellhouse et al. [15] pointed out that the zinc layer could be removed by using fuming HNO_3 , however it had been shown that the corrosion time was difficult to control due to its excessive corrosiveness in actual operation. Therefore, in this work, the surfaces of the specimens were wiped by absorbent cotton dipped in 38% HCl solution for about 3 to 4 s until the Fe–Al–Zn layer appears.

The Helios 600i focused ion beam (FIB, FEI, Waltham, MA, USA) is used to prepare specimens for the transmission electron microscope (TEM) to observe the microstructure of the interfacial layer between the zinc coating and the substrate. The zinc coating was stripped to let its thickness be controlled within 1 nm to facilitate ion beam cutting, and all specimens are protected by Pt plating. The JEOL-2100 field emission transmission electron microscope (Tokyo, Japan) was used in this work, the accelerating voltage was 200 kV, and the EDS energy spectrum beam spot size was 1 nm.

3. Experimental Results

3.1. Surface Structure of Samples Annealed at Different Annealing Temperatures

Figure 2 shows macroscopic-profiles of the galvanized surfaces of steel samples. The experimental dew point and H_2 content of the three samples were $-10\text{ }^\circ\text{C}$ and 20%, respectively, while the annealing temperatures were separately set as 873, 923 and 1093 K for sample 1#, 3# and 5#. It can be seen that the quality of the galvanized coating on the surface of sample 5# is far worse than the other two samples. The zinc coating on the surface of sample 1# is complete and smooth without obvious bare spot, as shown in Figure 2a. A small number of aggregated bare spots could be observed on the surface of sample 3#, of which the maximum diameter is about 3 mm, as shown in Figure 2b. It can be found

that the steel sheet will exhibit better galvanizability under the annealing process with lower annealing temperature by comparing three samples above.

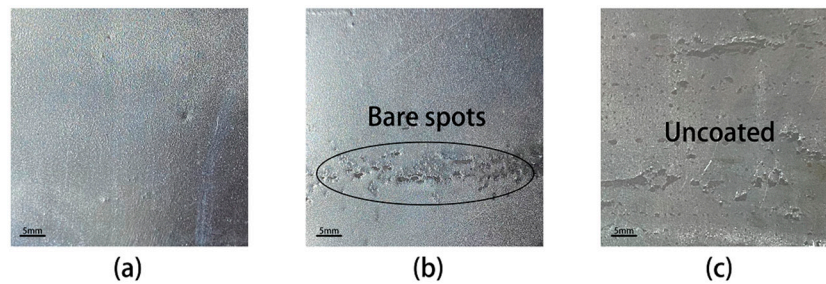


Figure 2. Surfaces of hot-dip galvanized samples annealed at different temperatures. (a) 1# (873 K), (b) 3# (923 K), (c) 5# (1093 K).

Figure 3 shows the SEM micrographs of surface oxides of samples 1#, 3# and 5#, respectively. It can be seen that the surface composition of specimens annealed at 873 K is close to that of the matrix, and there is almost no oxide formed on the surface. While shown in Figure 3b, fine oxide particles can be observed on the surface of sample 3#. When the annealing temperature rises to 1093 K, it can be observed that the size of the oxide particles on the surface of the sample 5# increases significantly, and a layer of obvious film-like oxide is formed, which covers the substrate surface. The EDS analyses in Figure 3 show that surface oxides of three samples are all MnO, and the content of manganese in the oxide layer increases from 5.5 to 30.6 wt.% with the increase in annealing temperature.

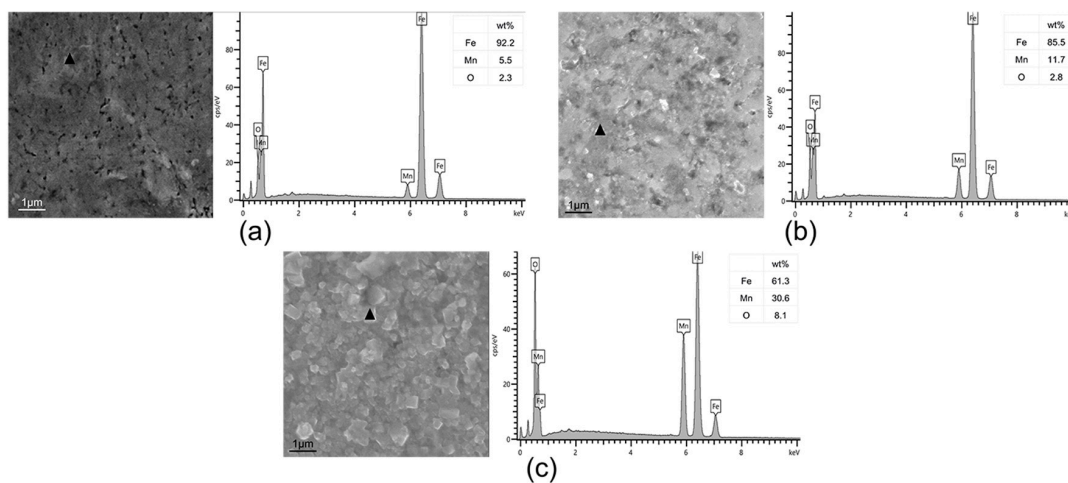


Figure 3. SEM micrographs and EDS analyses of surface oxides of samples annealed at different temperatures. (a) 1# (873 K), (b) 3# (923 K), (c) 5# (1093 K).

3.2. Surface Structure of Samples Annealed at Different Dew Points

Figure 4 shows macroscopic profiles of the galvanized surfaces of steel samples after annealing at 1093 K in the same reductive atmosphere of 20% H₂–80% N₂, but under different dew points (DP) as –50, –10 and +10 °C, respectively. The zinc coating is relatively uniform without large bare area formed on the surface of sample 4#, there are a small number of concentrated acicular bare spots instead, as shown in Figure 4a. In addition, for sample 5# annealed with –10 °C DP, there are a few zinc coatings on the surface, as shown in Figure 4b. When the dew point increases to +10 °C, it can be seen from Figure 4c that the coating quality of the sample 6# is seriously deteriorated for a large bare area exists in the sample surface.

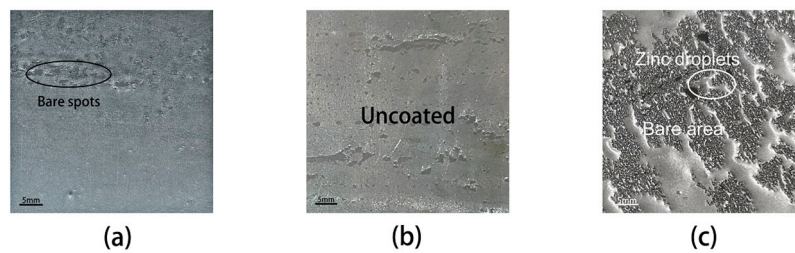


Figure 4. The surface of hot-dip galvanized samples annealed at different dew points. (a) 4# ($-50\text{ }^{\circ}\text{C}$), (b) 5# ($-10\text{ }^{\circ}\text{C}$), (c) 6# ($+10\text{ }^{\circ}\text{C}$).

Figure 5 shows the SEM micrographs of surface oxides of sample 4#, 5# and 6#. It is shown that as the dew point increases from -50 to $+10\text{ }^{\circ}\text{C}$, the size of the oxide particles on the surface of the samples increases significantly, and densely distributed film-like oxides are gradually formed. The oxide in Figure 5a is scattered on the surface of the substrate, while the oxide film in Figure 5c covers the entire substrate surface.

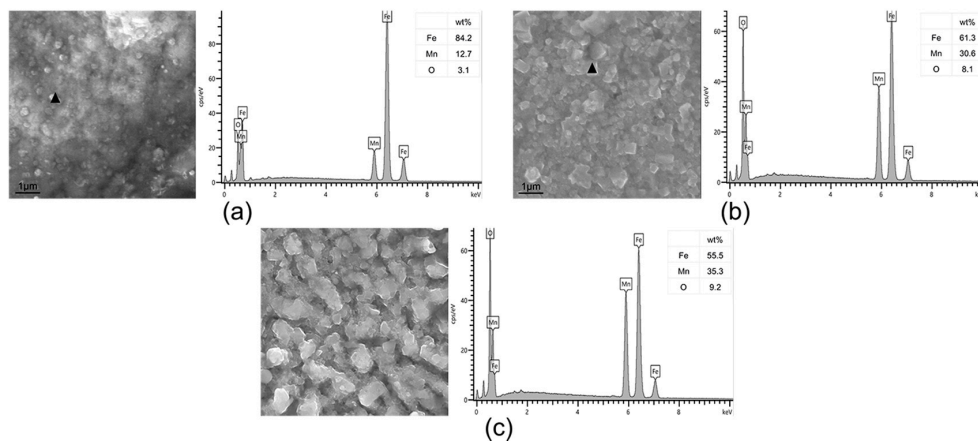


Figure 5. SEM micrographs and EDS analyses of surface oxides on the steel surface of samples annealed at different dew points. (a) 4# ($-50\text{ }^{\circ}\text{C}$), (b) 5# ($-10\text{ }^{\circ}\text{C}$), (c) 6# ($+10\text{ }^{\circ}\text{C}$).

3.3. Surface Microstructure in Different H_2 Content Atmospheres

Figure 6 shows macroscopic profiles of the galvanized surfaces of two medium Mn steel samples after having been annealed at 923 K under the same $-10\text{ }^{\circ}\text{C}$ DP but different reductive atmospheres of 5% H_2 and 20% H_2 , respectively. Concentrated pinhole-like bare spots distribute linearly in local area of both two samples. Morphologies of surface oxides on samples 2# and 3# are observed by SEM and EDS, as shown in Figure 7, the average diameter of surface oxide in sample 2# is bigger than that in sample 3#.

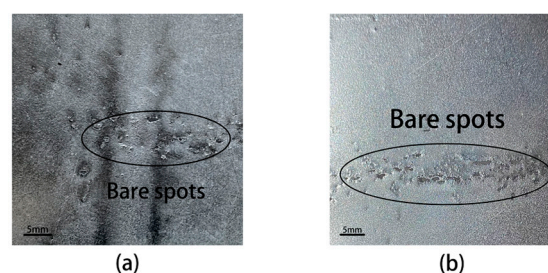


Figure 6. Surfaces of hot-dip galvanized samples annealed in different H_2 content atmospheres. (a) 2# (5% H_2), (b) 3# (20% H_2).

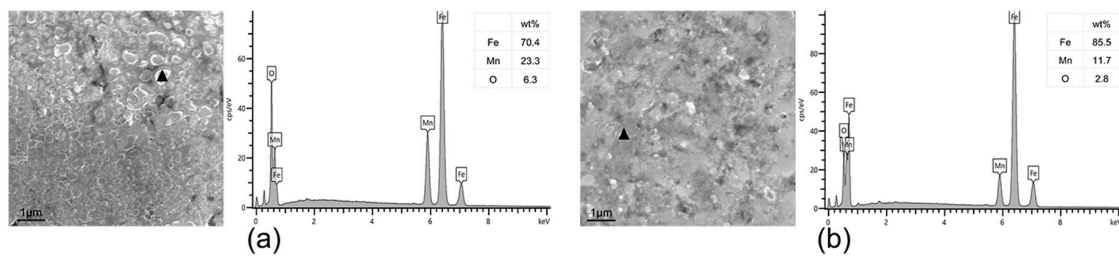


Figure 7. SEM micrographs and EDS analyses of surface oxides of samples annealed in different H₂ content atmospheres. (a) 2# (5% H₂), (b) 3# (20% H₂).

According to the above experimental analyses, the main type of oxide formed on the surfaces of experimental steel is MnO. With the increase in annealing temperature and dew point, the amount of oxides becomes more, while the contrary occurs when the H₂ content increases from 5% to 20%. It is difficult to find oxide particles on the surface of sample 1#. On the surfaces of samples 3#, 4# and 2#, oxide particles are relatively larger and more densely distributed, which leads to the tendency of aggregation into film-like oxides. On the surfaces of samples 5# and 6#, there are much larger film-like oxides.

Correspondingly, with the change of oxide morphology and distribution, the zinc coating quality of the experimental steel samples is different. Sample 1# with a few oxides has no defects of bare spots. Relatively larger oxide particles lead to pinhole-like bare spots on the surface of samples 3#, 4# and 2#. When a dense layer of oxide film is formed on the surface of 5# and 6# samples, a large area of bare area appears which means a serious deterioration of coating quality.

4. Discussion

4.1. Thermodynamic Analysis on the Oxide Formation of Experimental Steel during Annealing

The formation of oxides on experimental steel was thermodynamically analyzed based on the work of Suzuki et al. [16]. According to Suzuki et al., it was assumed that local thermodynamic equilibrium was established between the oxide layer and metal ion diffusion layer of experimental steel during the annealing process. In calculation, the thermodynamic data of ferrite, austenite as well as oxide phases are provided by the databases TCFE9 and SSUB6 in the commercial software Thermo-Calc (Version: 2018b), respectively. All the oxide reactions in the calculation are considered to be taking place during high temperature annealing because the dipping time in the Zn bath is very short.

Based the on previous study [14], for aluminum-containing light steel, the oxygen partial pressure is the major factor that determines the type and morphology of oxides on the surface of the steel samples. In present work, according to Formulas (1) and (2) [17], the oxygen potential corresponding to annealing process can be obtained as shown in Table 2.

$$\log P(\text{O}_2) = 6.00 - \frac{26176}{T} + 2 \log [P_{\text{sat}}(\text{H}_2\text{O})/P(\text{H}_2)] \quad (1)$$

where T is the annealing temperature (K); $P(\text{H}_2)$ is the partial pressure of hydrogen; $P_{\text{sat}}(\text{H}_2\text{O})$ is the saturated vapor pressure of H₂O.

The well-known equation for $P_{\text{sat}}(\text{H}_2\text{O})$ (saturated water vapor pressure) and DP follows:

$$\frac{1}{2} \log P_{\text{sat}}(\text{H}_2\text{O}) = \begin{cases} \frac{9.8DP}{273.15+DP} - \frac{13088}{T} - \log P(\text{H}_2) + 0.78 & DP \leq 0^\circ\text{C} \\ \frac{7.58DP}{240+DP} - \frac{13088}{T} - \log P(\text{H}_2) + 0.78 & DP > 0^\circ\text{C} \end{cases} \quad (2)$$

Table 2. Oxygen partial pressures at different annealing conditions.

No.	$P(O_2)/atm$
1#	1.72×10^{-28}
3#	7.24×10^{-27}
4#	4.28×10^{-26}
2#	1.16×10^{-25}
5#	1.86×10^{-22}
6#	4.16×10^{-21}

Combining the calculation results of oxygen partial pressure and experimental results of oxide formation on steel samples, it is not difficult to find that as $P(O_2)$ increases, the surface oxidation of the experimental steel becomes obvious. In order to further analyze the oxidation behavior of steel samples during the annealing process, the type and content of oxides corresponding to different oxygen partial pressures are thermodynamically calculated, as shown in Figure 8.

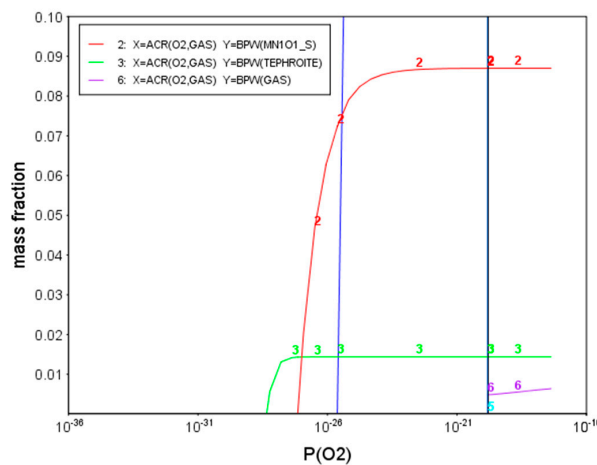


Figure 8. Variation of the formation of oxide with oxygen potential pressure obtained by thermodynamic calculation.

As shown in Figure 8, the mass fraction of oxide formed on the surface of each sample can be obtained, and then the content of oxide can be compared in Figure 9. It is shown that with the oxygen partial pressure rising, the oxide firstly formed is Mn_2SiO_4 (TEPHROITE) and subsequently MnO . Moreover, the mass fraction of the two oxides will also increase with the increase in oxygen partial pressure, and the content of MnO is much greater than that of Mn_2SiO_4 .

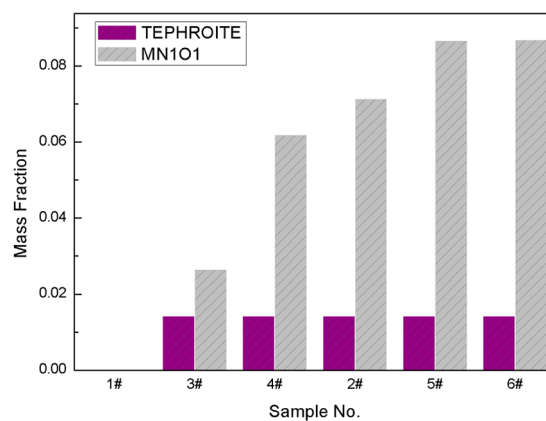


Figure 9. Comparison of the content of oxide on the samples according to thermodynamic calculation.

It is clear in Figure 9, there would be no oxide formation on the surface of sample 1#, while the amount of manganese oxides formed on the surface of samples 3#, 4# and 2# increases as oxygen partial pressure changes from 7.24×10^{-27} to 1.16×10^{-25} atm. Under the oxygen partial pressure of 1.86×10^{-22} and 4.16×10^{-21} atm for samples 5# and 6#, it can be seen that the amount of oxides on the surface of these two samples reaches the maximum. The presence of a large number of stable oxides would form oxide layers. Moreover, as pointed by many authors [11,18,19], film-like MnO is more likely to cause surface defects with a deterioration of the quality of zinc coating than that of granulated oxide.

In addition, according to the EDS analysis of the surfaces of steel samples shown in Figures 3, 5 and 7, the manganese contents under different oxygen partial pressures can be obtained, as shown in Table 3.

Table 3. EDS analyses results of manganese contents on the surfaces of 1#–6# samples.

Sample No.	$P(\text{O}_2)/\text{atm}$	Manganese Content/wt.%
1#	1.72×10^{-28}	5.5
3#	7.24×10^{-27}	11.7
4#	4.28×10^{-26}	12.7
2#	1.16×10^{-25}	23.3
5#	1.86×10^{-22}	30.6
6#	4.16×10^{-21}	35.3

It is shown that with the increase in oxygen partial pressures, the content of manganese becomes higher correspondingly. It is not difficult to find out that under the condition of higher oxygen partial pressure, the enrichment of manganese on the surface is more obvious, resulting in the higher content of MnO formed. It should be noted that there is no silicon enrichment on the surface which probably caused by the low content of 0.2 wt.% Si in the steel matrix. Therefore, although the Mn_2SiO_4 is also thermodynamic stable, the Mn–Si–O complex oxide is difficult to form on the surface of steel sample.

4.2. Analysis of Interfacial Microstructure of Experimental Steel

The result of the thermodynamic calculation shows that the oxides of experimental steel are composed of MnO and Mn_2SiO_4 . Moreover, the amount of oxide increases with the increase in oxygen partial pressure. In addition, the amount of MnO is much larger than that of Mn_2SiO_4 , and the Mn–Si–O complex oxide is difficult to form on the surface of steel sample. As is well known, when the steel is dipped in the zinc bath, MnO and Mn_2SiO_4 can react with aluminum in liquid zinc (aluminothermic reduction). Obviously, in order to reduce a large number of oxides, more aluminum would be consumed which hinders the formation of an Fe–Al–Zn intermetallic compound and leads to the formation of Fe–Zn brittle phases. A good zinc coating would be obtained while there is a continuous distributed inhibition layer formed on the surface of steels. If a large amount of oxides are formed on the surface of the steel sheet, it will prevent the zinc liquid from contacting the steel sheet, which is not conducive to the formation of the inhibition layer. Therefore, the inhibition layers of the six samples were analyzed in order to further clarify the formation of surface oxides of experimental steel under different oxygen partial pressures.

Figure 10 shows the microstructures of the inhibition layer of all six samples. For sample 1# under the lowest oxygen partial pressure, the inhibition layer at the steel substrate/Zn coating interface is composed of regular cubic crystals of an Fe–Al–Zn intermetallic compound with a thickness of only tens to hundreds of nanometers, which can effectively hinder the formation of Fe–Zn brittle phases and improve the adhesion of the coating for sample 1#. There are coarsened inhibition layer particles which appear on the surfaces of samples 3#, 4# and 2#, which are still finely and tightly distributed, and thus there is no large area of bare spot defect, as shown in Figure 10b–d. The distribution of the inhibition layer of samples 5# and 6# under higher oxygen partial pressure is discontinuous, so that

the coverage of the inhibition layer is significantly lower than that of the other four samples stated above, especially for sample 6# under the highest oxygen partial pressure, where a large area of the bare matrix can be seen on the surface.

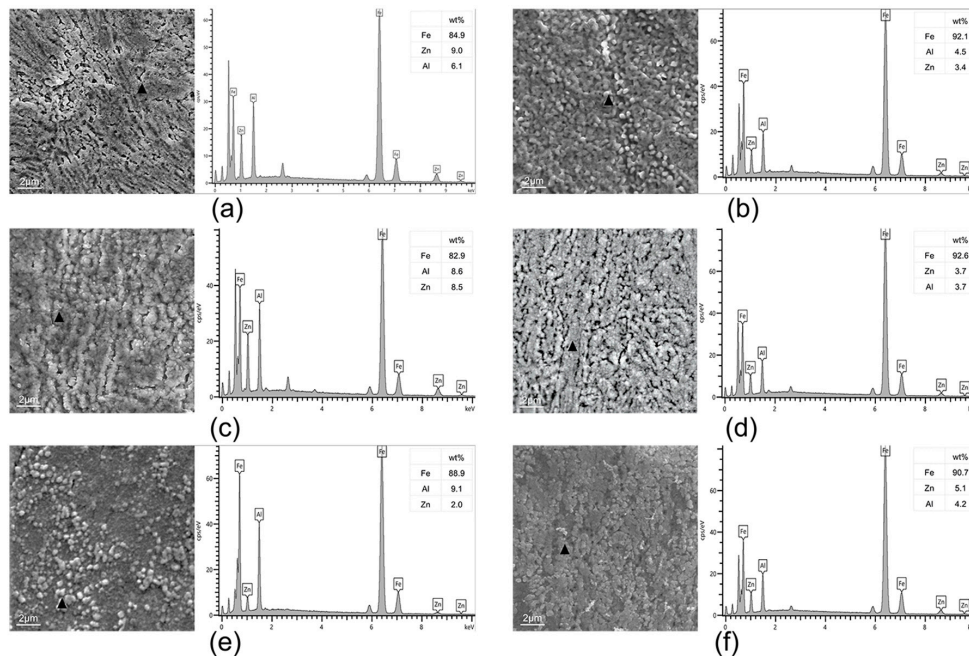


Figure 10. SEM micrographs and EDS analyses of the inhibition layer on the steel/coating interfaces of all samples. (a) 1#, (b) 3#, (c) 4#, (d) 2#, (e) 5#, (f) 6#.

According to the analysis above, it is not difficult to find that with the increase in the oxygen partial pressure, the amount of oxides increases, and the particle size of the inhibition layer on the surface of the steel continues to coarsen, which leads to a decrease in the coverage of the inhibition layer. To further investigate the effect of surface oxide on the zinc coating layer, the interface microstructure between the Zn coating/Fe substrates of samples 1#, 4#, 5# and 6# under different oxygen partial pressures were analyzed by transmission electron microscopy. The results are shown in Figures 11–14.

Figure 11 shows TEM analysis of the coating/substrate interface of sample 1# under the 1.72×10^{-28} oxygen partial pressure. It can be seen from the element distribution in Figure 11a,b that the entire cross-section is composed of a zinc layer, inhibition layer and matrix. The fine particles of the $\text{Fe}_2\text{Al}_5\text{Zn}_{0.5}$ inhibition layer are uniformly and tightly distributed on the surface to form a good inhibition layer with a thickness of about 116 nm. A very small amount of fine MnO particles are distributed above the inhibition layer, with a diameter of about 78 nm. When combined with the thermodynamic calculation results in Figure 8, MnO is not a thermodynamic stable phase, so it contains a negligible amount.

Figure 12 shows TEM analysis of the coating/substrate interface of sample 4# under 4.28×10^{-26} oxygen partial pressure. The thickness of the inhibition layer of sample 4# is about 113 nm, which is almost the same as that of sample 1#. However, as shown in Figure 12c, MnO particles formed in sample 4# are coarser than those in sample 1#, and its diameter is about 120 nm. MnO particles with bigger size are formed in the $\text{Fe}_2\text{Al}_5\text{Zn}_{0.4}$ inhibition layer, thereby hindering the continuous distribution of the inhibition layer and causing the bare area on the surface. In addition, consistent with the prediction of thermodynamic calculation, a small amount of Mn_2SiO_4 oxide can be found beside the steel substrate, as shown in Figure 12e, which has little effect on galvanizability.

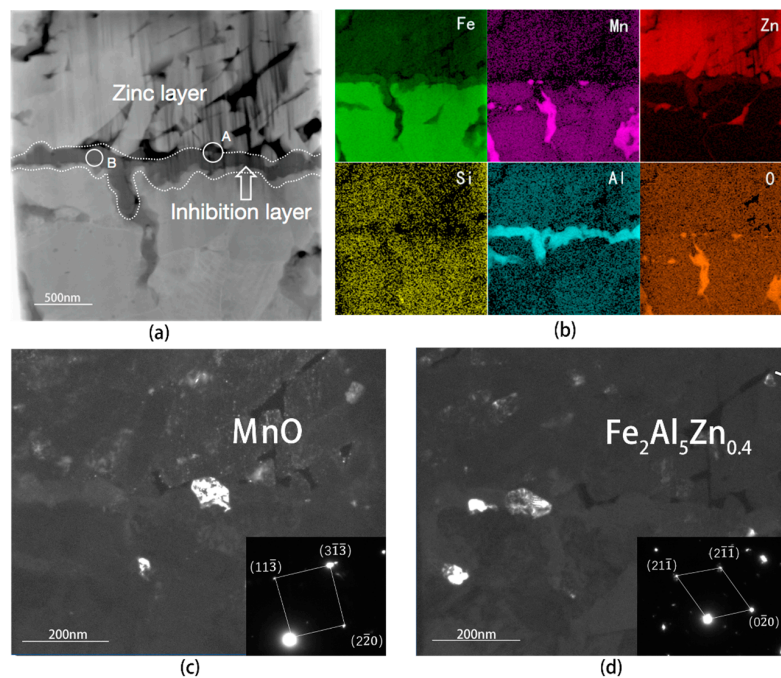


Figure 11. (a) TEM analysis of the Zn coating/Fe substrate interface of the galvanized sample1#. (b) cross-sectional elemental maps of the area. (c) Dark filed image and diffraction pattern of the oxide particle corresponding to zone A in (a). (d) Dark filed image and diffraction pattern of the inhibition layer corresponding to zone B in (a).

Figure 13 shows TEM analysis of the coating/substrate interface of sample 5# under 1.86×10^{-22} oxygen partial pressure. It can be seen from Figure 13a that MnO oxide particles on the surface are coarsened and aggregated, so there is a tendency to form film-like oxides in local areas. The size of manganese oxide particles is further increased, with a diameter of about 182 nm, as shown in Figure 13c. Under the manganese oxide layer, there are abnormally grown grains with a size of about 500 nm in the inhibition layer. Large particles of Mn_2SiO_4 oxide with a size of about 190 nm are formed in the Fe substrate. In addition, it can be observed that an Fe–Al–Zn intermetallic compound is formed at the grain boundaries and extended into the Fe substrate, and the Fe–Zn intermetallic compound is adjacent to $Fe_2Al_5Zn_{0.4}$ layer. These results indicate that the zinc liquid could penetrate into the iron substrate, and part of the Fe–Al–Zn phase transform into an Fe–Zn phase due to the depletion of Al participating in aluminothermic reduction [20], the reaction equation is as follows:

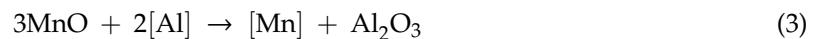


Figure 14 shows TEM analysis of the coating/substrate interface of sample 6# under 4.16×10^{-21} oxygen partial pressure. The surface manganese oxide particles are further coarsened, with a size of about 420 nm, forming a dense MnO oxide layer on the surface with a thickness of about 450 nm, which cannot be reduced by the aluminothermic reduction. The surface film-like oxides completely block the contact between the zinc liquid and the substrate, so there is almost no formation of inhibition layer. Meanwhile, Mn_2SiO_4 is also found in the steel substrate due to the enrichment of silicon on the steel surface.

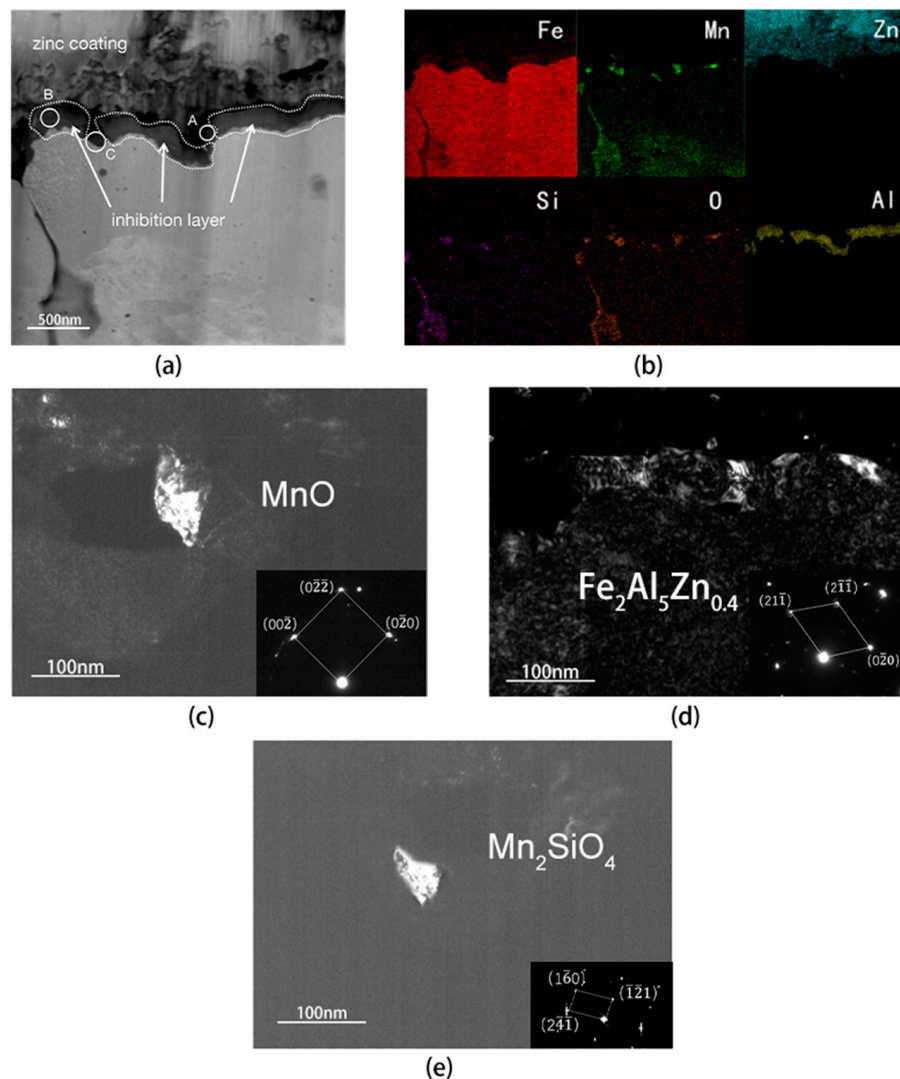


Figure 12. (a) TEM analysis of the Zn coating/Fe substrate interface of the galvanized sample 4#. (b) cross-sectional elemental maps of the area shown in (a). (c) Dark filed image and diffraction pattern of the oxide particle corresponding to zone A in (a). (d) Dark filed image and diffraction pattern of the inhibition layer corresponding to zone B in (a). (e) Dark filed image and diffraction pattern of the oxide particle corresponding to zone C in (a).

According to the above analysis results, it is not difficult to find that the galvanizability of experimental steel with the lowest dew point (sample 4#) or the highest dew point (sample 6#) is not the best, while the galvanizability of the steel (sample 2#) with the lowest H_2 content is not the worst, and the annealing temperature also cannot determine the galvanizability. The effect of annealing process parameters on the galvanizability of experimental steel can be comprehensively evaluated using oxygen partial pressure. For the experimental steel, it is shown that under a low oxygen partial pressure of about 10^{-28} atm, manganese oxide particles in the form of the metastable phase are formed on the surface in a small amount and the inhibition layer is uniformly and tightly distributed on the surface, and then the ideal galvanizability of steel can be acquired. As the oxygen partial pressure increases to higher than 10^{-25} atm, the manganese oxide particles are thermodynamic stable. So, its precipitation constantly enlarges and aggregates on the surface, distributing continuously and tending to form an oxide film. When the oxygen partial pressure is greater than 10^{-22} atm, the equilibrium phase content of MnO is obviously higher than other samples. It is difficult for the aluminothermic reduction to

reduce a large number of manganese oxides, these film-like MnO hinder the formation of the inhibition layer and deteriorate the galvanizability. Based on the above discussion, it is shown that the dew point, the annealing temperature and H_2 content can be regulated to reach a condition below 10^{-28} oxygen partial pressure, the solution of ideal galvanizability of medium manganese steel can be obtained.

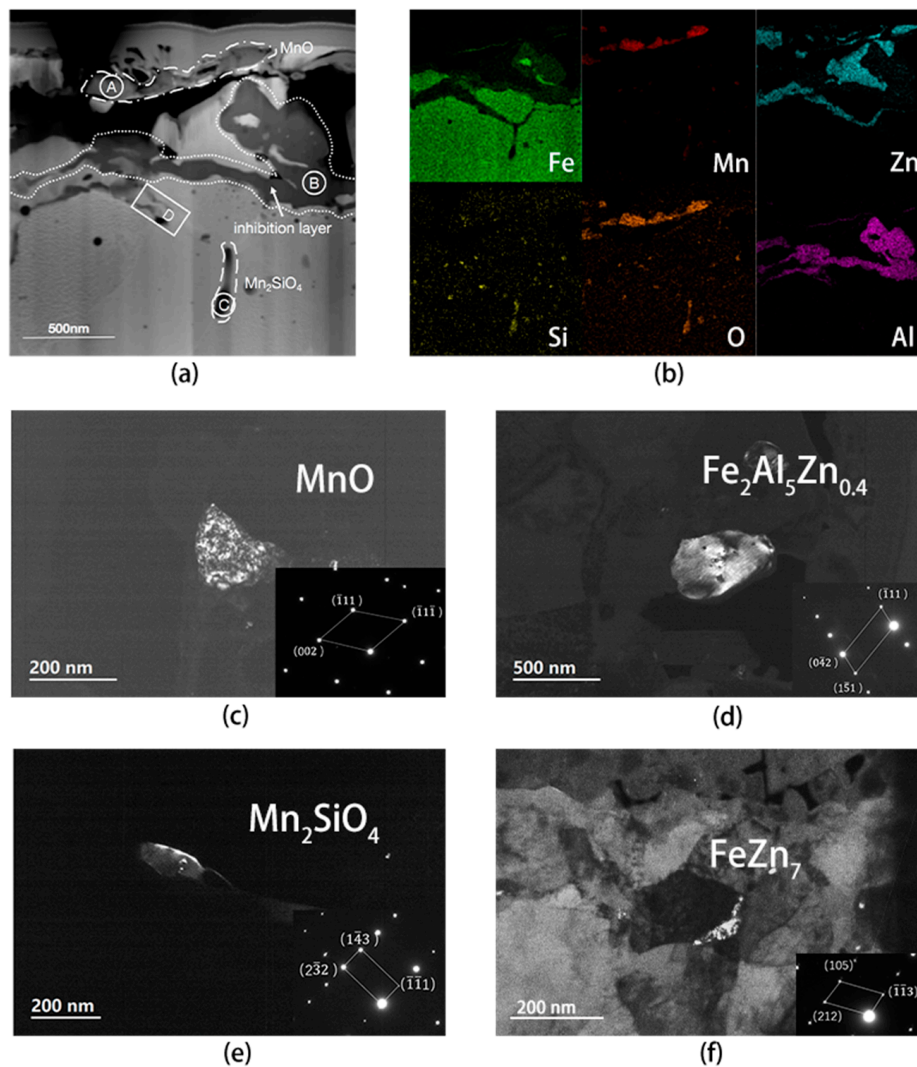


Figure 13. (a) TEM analysis of the Zn coating/Fe substrate interface of the galvanized sample 5#. (b) cross-sectional elemental maps of the area shown in (a). (c) Dark field image and diffraction pattern of the oxide particle corresponding to zone A in (a). (d) Dark field image and diffraction pattern of the inhibition layer corresponding to zone B in (a). (e) Dark field image and diffraction pattern of the oxide particle corresponding to zone C in (a). (f) Dark field image and diffraction pattern of the Fe-Zn intermetallic corresponding to zone D in (a).

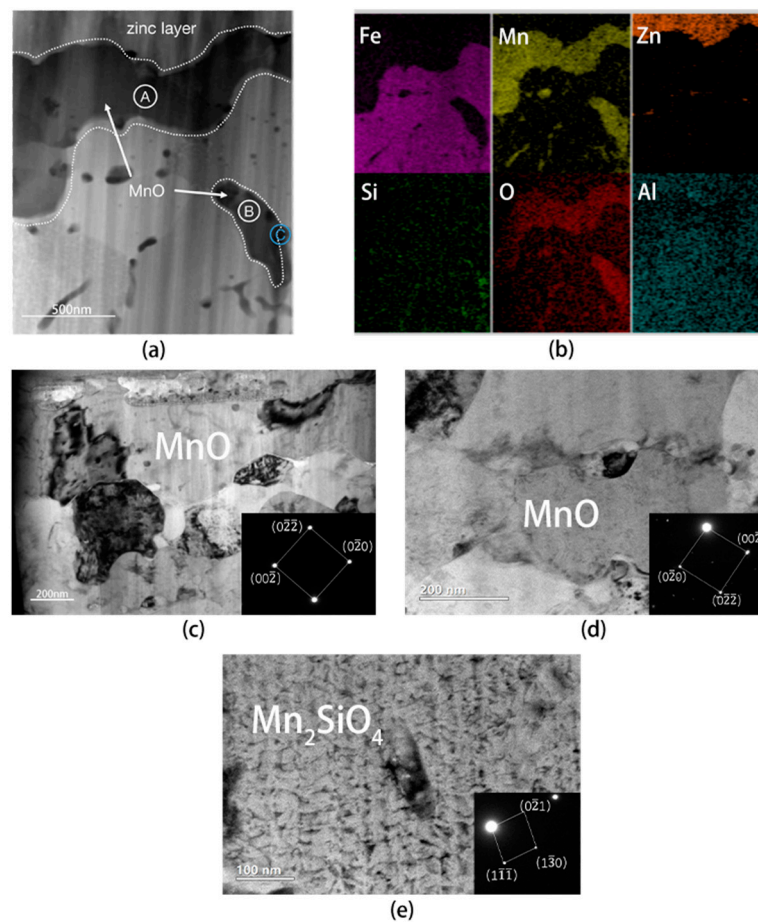


Figure 14. (a) TEM analysis of the Zn coating/Fe substrate interface of the galvanized sample 6#. (b) cross-sectional elemental maps of the area shown in (a). (c) Bright filed image and diffraction pattern of the oxide particle corresponding to zone A in (a). (d) Bright filed image and diffraction pattern of the oxide particle corresponding to zone B in (a). (e) Bright filed image and diffraction pattern of the oxide particle corresponding to zone C in (a).

5. Conclusions

Based on thermodynamic analysis of oxide formation in the annealing process, the oxygen partial pressure $P(O_2)$ can be used to comprehensively evaluate the effects of dew point, annealing temperature and annealing atmosphere on the surface oxidation of steel samples. Under different annealing conditions, the thermodynamic stable oxides formed on the experimental steel are consistently MnO and Mn_2SiO_4 , and the content of MnO is much higher. As oxygen partial pressure increases, there is an enhancement of equilibrium precipitation of MnO accordingly.

With the increase in oxygen partial pressure, the content of manganese in the steel surface increases correspondingly. During the annealing, the formation of MnO is caused by the enrichment of manganese towards surface. However, since there is no enrichment of silicon on the steel surface, it is difficult to form a Mn–Si–O composite oxide. Composite oxides are generally formed in the Fe substrate and have little effect on the galvanizability.

When the value of oxygen partial pressure is about 10^{-28} atm, there is no thermodynamic stable oxide, the ideal galvanizability of steel can be obtained because its continuous inhibition layer distributes on the surface. As $P(O_2)$ increases over 10^{-25} atm, MnO is a thermodynamic stable phase. The oxide particles become coarser with a rise in their number and tend to aggregate, which has an adverse effect on the formation of a continuous inhibition layer, resulting in the defects of bare spots on the surface of the steel. When the oxygen partial pressure is greater than 10^{-22} atm, a film-like

MnO layer is formed on the surface of steel sample, which obviously deteriorates the galvanizability. The galvanizability of the steel can be improved by the regulation of oxygen partial pressure, therefore, the reasonable zinc plating process parameters can be developed.

Author Contributions: Conceptualization, Y.H. and Z.C.; methodology, Y.H.; software, Z.C.; validation, Z.C.; formal analysis, H.W.; investigation, Z.C.; resources, Y.H.; data curation, W.Z.; writing—original draft preparation, Z.C.; writing—review and editing, Z.C.; visualization, Y.Z.; supervision, L.L.; project administration, Y.H.; funding acquisition, Y.H. All authors have read and agreed to the published version of the manuscript.

Funding: This work is financially supported by the National Key R&D Program of China (2017YFB0304402) and the National Natural Science Foundation of China (51971127).

Conflicts of Interest: The authors declare no conflict of interest.

References

1. Luo, H.W.; Shi, J.; Wang, C. Experimental and numerical analysis on formation of stable austenite during the intercritical annealing of 5Mn steel. *Acta Mater.* **2011**, *5*, 4002–4014. [[CrossRef](#)]
2. Xu, H.-F.; Zhao, J.; Cao, W.; Shi, J.; Wang, C.; Li, J.; Dong, H.; Wang, C. Heat treatment effects on the microstructure and mechanical properties of a medium manganese steel (0.2C–5Mn). *Mater. Sci. Eng. A* **2012**, *532*, 435–442. [[CrossRef](#)]
3. Wang, C.; Cao, W.Q.; Hang, Y. Influences of austenization temperature and annealing time on duplex ultrafine microstructure properties of medium Mn steel. *J. Iron Steel Res. Int.* **2015**, *22*, 42–47. [[CrossRef](#)]
4. Cho, L.; Jung, G.S.; Cooman, B.C.D. On the transition of internal to external selective oxidation on CMnSi TRIP steel. *Metall. Mater. Trans. A* **2014**, *45*, 5158–5172. [[CrossRef](#)]
5. Seyed Mousavi, G.; Mcdermid, J.R. Selective oxidation of a C–2Mn–1.3Si (wt pct) advanced high-strength steel during continuous galvanizing heat treatments. *Metall. Mater. Trans. A* **2018**, *49*, 1–15. [[CrossRef](#)]
6. Samanta, S.; Halder, A.K.; Deo, Y. Effect of Mn and Cr on the selective oxidation, surface segregation and hot-dip Zn coatability. *Surf. Coat. Technol.* **2019**, *377*, 1–9. [[CrossRef](#)]
7. Yonggang, D.; Hongshuang, D.; Misra, R.D.K. Influence of dew point on the selective oxidation, microstructure and mechanical properties of a high-Al low-Si dual phase steel during hot-dip galvanizing process. *Prot. Met. Phys. Chem. Surf.* **2018**, *54*, 496–502.
8. Staudte, J.; Maigne, J.M.; Del Frate, F. Optimizing the manganese and silicon content for hot dip galvanizing of 3rd generation advanced high strength steels. *Metall. Res. Technol.* **2014**, *111*, 17–23. [[CrossRef](#)]
9. Maderthaner, M.; Jarosik, A.; Angeli, G.; Haubner, R. Effect of dew point on the selective oxidation of advanced high strength steels. *Mater. Sci. Forum* **2017**, *891*, 292–297. [[CrossRef](#)]
10. Mousavi, G.S.; Mcdermid, J.R. Effect of dew point on the reactive wetting of a C–2Mn–1.3Si(wt%) advanced high strength steel during continuous galvanizing. *Surf. Coat. Technol.* **2018**, *351*, 11–20. [[CrossRef](#)]
11. Pourmajidian, M.; Mcdermid, J.R. Selective oxidation of a 0.1C–6Mn–2Si third generation advanced high-strength steel during dew-point controlled annealing. *Metall. Mater. Trans. A* **2018**, *49*, 1795–1808. [[CrossRef](#)]
12. Pourmajidian, M.; Mcdermid, J.R. Effect of annealing temperature on the selective oxidation and reactive wetting of a 0.1C–6Mn–2Si advanced high strength steel during continuous galvanizing heat treatments. *ISIJ Int.* **2018**, *58*, 1635–1643. [[CrossRef](#)]
13. Pourmajidian, M.; McDermid, J.R. On the reactive wetting of a medium-Mn advanced high-strength steel during continuous galvanizing. *Surf. Coat. Technol.* **2019**, *357*, 418–426. [[CrossRef](#)]
14. Yang, T.; He, Y.; Chen, Z.; Zheng, W.; Wang, H.; Li, L. Effect of dew point and alloy composition on reactive wetting of hot dip galvanized medium manganese lightweight steel. *Coatings* **2020**, *10*, 37. [[CrossRef](#)]
15. Bellhouse, E.M.; McDermid, J.R. Analysis of the Fe–Zn interface of galvanized high Al–low Si TRIP steels. *Mater. Sci. Eng. A* **2008**, *491*, 39–46. [[CrossRef](#)]
16. Suzuki, Y.; Sugimoto, Y.; Yamashita, T.; Fujita, S.; Yamaguchi, S. Thermodynamic analysis of selective oxidation behavior of Si and Mn-added steel during recrystallization annealing. *ISIJ Int.* **2009**, *49*, 564–573. [[CrossRef](#)]
17. Huachu, L.; Yanlin, H.; Lin, L. Application of thermodynamics and Wagner model on two problems in continuous hot-dip galvanizing. *Appl. Surf. Sci.* **2009**, *256*, 1399–1403.

18. Alibeigi, S.; Kavitha, R.; Meguerian, R.J.; McDermid, J.R. Reactive wetting of high Mn steels during continuous hot-dip galvanizing. *Acta Mater.* **2011**, *59*, 3537–3549. [[CrossRef](#)]
19. Kim, Y.; Shin, K.-S.; Jeon, S.-H.; Chin, K.-G.; Lee, J. The influence of the dew point on the wettability of twinning-induced-plasticity steels by liquid Zn–0.23-wt% Al. *Corros. Sci.* **2014**, *85*, 364–371. [[CrossRef](#)]
20. Khondker, R.; Mertens, A.; McDermid, J.R. Effect of annealing atmosphere on the galvanizing behavior of a dual-phase steel. *Mater. Sci. Eng. A* **2007**, *463*, 157–165. [[CrossRef](#)]

Publisher’s Note: MDPI stays neutral with regard to jurisdictional claims in published maps and institutional affiliations.



© 2020 by the authors. Licensee MDPI, Basel, Switzerland. This article is an open access article distributed under the terms and conditions of the Creative Commons Attribution (CC BY) license (<http://creativecommons.org/licenses/by/4.0/>).